AD-A044 559 NAVAL OCEAN SYSTEMS CENTER SAN DIEGO CALIF F/G 3/2
EMISSION AND ABSORPTION AT WAVELENGTHS OF 8.6 MM AND 2.0 CM AS --ETC(U)
JUL 77 M P BLEIWEISS, F L WEFER, A E KONIGES

UNCLASSIFIED NOSC/TR-136 NL


END
DATE FILMED
10-77
DDC

(12)

# NOSC

NOSC / TR 136

NOSC / TR 136

**Technical Report 136**

# EMISSION AND ABSORPTION AT WAVELENGTHS OF 8.6 mm AND 2.0 cm AS DETERMINING FACTORS OF $T_e$ AND $N_e$ IN THE FILAMENT

MP Bleiweiss, FL Wefer, and AE Koniges

17 July 1977

Research and Development, December 1973 to July 1977

Prepared for
National Aeronautics and Space Administration



Approved for public release; distribution is unlimited

NAVAL OCEAN SYSTEMS CENTER
SAN DIEGO, CALIFORNIA 92152

NAVAL OCEAN SYSTEMS CENTER, SAN DIEGO, CA 92152

AN ACTIVITY OF THE NAVAL MATERIAL COMMAND

RR GAVAZZI, CAPT, USN
Commander

HOWARD L BLOOD, PhD
Technical Director

## ADMINISTRATIVE INFORMATION

Work was performed under FGOV, O, NASA (M229), by members of the staff of La Posta Astrogeophysical Observatory. The report covers work from December 1973 to July 1977 and was approved for publication 17 July 1977.

Released by
JH Richter, Head
EM Propagation Division

Under authority of
JD Hightower, Head
Environmental Sciences Department

UNCLASSIFIED

SECURITY CLASSIFICATION OF THIS PAGE (When Data Entered)

| REPORT DOCUMENTATION PAGE | | READ INSTRUCTIONS BEFORE COMPLETING FORM |
|---|---|---|
| 1. REPORT NUMBER<br>NOSC Technical Report 136 (TR 136) | 2. GOVT ACCESSION NO. | 3. RECIPIENT'S CATALOG NUMBER<br>NOSC/TR-136 |
| 4. TITLE (and Subtitle)<br>Emission and Absorption at Wavelengths of 8.6 mm and 2.0 cm as Determining Factors of $T_e$ and $N_e$ in the Filament. | | 5. TYPE OF REPORT & PERIOD COVERED<br>Research and Development rept.<br>December 1973 ⇔ July 1977<br>6. PERFORMING ORG. REPORT NUMBER |
| 7. AUTHOR(s)<br>MP Bleiweiss, FL Wefer, and AE Koniges | | 8. CONTRACT OR GRANT NUMBER(s) |
| 9. PERFORMING ORGANIZATION NAME AND ADDRESS<br>Naval Ocean Systems Center<br>San Diego, CA 92152 | | 10. PROGRAM ELEMENT, PROJECT, TASK AREA & WORK UNIT NUMBERS<br>FGOV, O, NASA (M229) |
| 11. CONTROLLING OFFICE NAME AND ADDRESS<br>National Aeronautics and Space Administration<br>Marshall Space Flight Center<br>Huntsville, AL 35801 | | 12. REPORT DATE<br>17 July 1977<br>13. NUMBER OF PAGES<br>48 (12) 24 |
| 14. MONITORING AGENCY NAME & ADDRESS (if different from Controlling Office) | | 15. SECURITY CLASS. (of this report)<br>Unclassified<br>15a. DECLASSIFICATION/DOWNGRADING SCHEDULE |

16. DISTRIBUTION STATEMENT (of this Report)

Approved for public release; distribution is unlimited

17. DISTRIBUTION STATEMENT (of the abstract entered in Block 20, if different from Report)

18. SUPPLEMENTARY NOTES

19. KEY WORDS (Continue on reverse side if necessary and identify by block number)

Solar emissions
Solar prominences

20. ABSTRACT (Continue on reverse side if necessary and identify by block number)

Observations of filaments at radio wavelengths show them as depressions against a quiet solar background. Until recently, simple models have been used to explain these observations. More detailed models have been developed and these are discussed together with past efforts at solar observations in order to better define these filaments.

DD FORM 1 JAN 73 1473 EDITION OF 1 NOV 65 IS OBSOLETE

393159

UNCLASSIFIED

SECURITY CLASSIFICATION OF THIS PAGE (When Data Entered)

## OBJECTIVE

Investigate the generation and progression of radio filaments across the solar disc. Develop models for analyses of the behavior of such emissions.

## RESULTS

Models for determination of the characteristics of filament behavior at wavelengths of 8.6 mm and 2.0 cm were developed and calculations were made which yielded reasonable temperature and electron-density parameters.

## RECOMMENDATION

Conduct a more extensive analytical study of radio filament behavior using radioheliograms obtained at the La Posta Astrogeophysical Observatory.

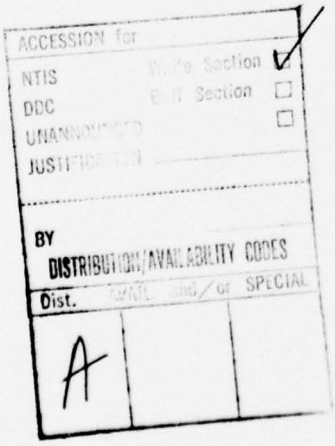

## CONTENTS



## ILLUSTRATIONS



## TABLE

## INTRODUCTION

Observations of filaments at radio wavelengths have been presented by a number of authors.[1-3] Disc observations of radio filaments show them as depressions against the quiet background; in other words, they are seen in absorption. Also there have been some observations of filaments (prominences) in emission.[2] Until recently, simple models have been used to explain the observations; however, there are three recent papers which present more detailed models.[4-6] While it was with respect to the simple models that the present analysis was originally proposed, the new models will also be discussed. This report reviews past efforts and attempts to use some unique observations obtained at the La Posta Astrogeophysical Observatory (LPAO) to better "define" radio filaments. These observations are unique in that the same filament/prominence has been seen at two frequencies in both emission and absorption.

First, the data are presented and parameters useful for model development are tabulated. Next, the simple models are discussed and the relevancy of our observations to the new models is shown. We end with conclusions and suggestions for future work.

## DATA

During the end of November and the first part of December 1973, a large filament was seen to traverse the solar disc. The optical observations of the filament presented here were obtained from the Sacramento Peak Observatory. At radio wavelengths, the filament was seen as a depression or "absorption" feature while on the disc, and usually in emission while on the west limb. These radio observations were made at LPAO as part of a solar monitoring program where radiospectroheliograms at 8.6-mm and 2.0-cm wavelengths are acquired daily. Although data have been collected since August 1972, the present case is the only obvious observation of a filament in emission.

The radio maps are acquired by scanning the sun in a square boustrophendonic raster containing 35 by 35 points at 8.6 mm and 19 by 19 points at 2.0 cm. The grid spacing is 1.0 and 2.0 arcmin, and data acquisition requires about 60 minutes and 25 minutes at 8.6 mm and 2.0 cm, respectively. Each map is calibrated by standard techniques; however, due to varying atmospheric attenuation and system gain changes, the data have had to be normalized to provide consistent results.[7] The normalization has resulted in a background level (assumed constant in time) which does not vary more than ±1% from map to map. This makes possible comparisons of features from one day to the next with a high degree of accuracy. Sample maps obtained at each wavelength are shown in figures 1 and 2. The temperature contours are in percent of the central disc antenna temperature; the interval between contours is 1% near the disc center.

The antenna pattern produces smoothing of the radio brightness distribution such that features away from the disc center become "hidden." To compensate for this, an average map has been constructed and subtracted from individual maps to produce differenced maps. An example of such a differenced map is shown in figure 3. Due to the varying solar angular

1. Khangil'din, UV, Soviet Astronomy-AJ, 8, p 234-242, 1964
2. Kundu, MR, Solar Physics, 25, p 108-115, 1972
3. Kundu, MR, and McCullough, TP, Solar Physics, 24, p 133-141, 1972
4. Straka, RM, Papagiannis, MD, and Kogut, JA, Solar Physics, 45, p 131-149, 1975
5. Chiuderi-Drago, F, Furst, E, Hirth, W, and Lantos, P, Astronomy and Astrophysics, 39, p 429-435, 1975
6. Butz, M, Furst, E, Hirth, W, and Kundu, MR, Solar Physics, 45, p 125-129, 1975
7. Megatek Corporation Report R2005-031-IF-3, by FL Wefer, 5 April 1976

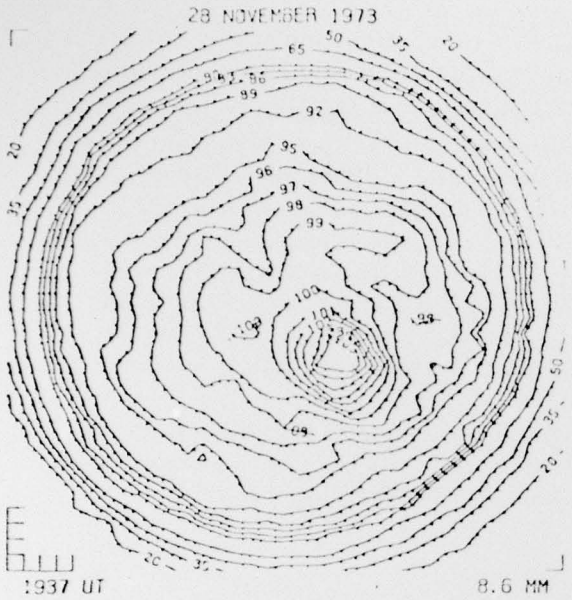


Figure 1. Radio map at 8.6 mm (1937 UT).

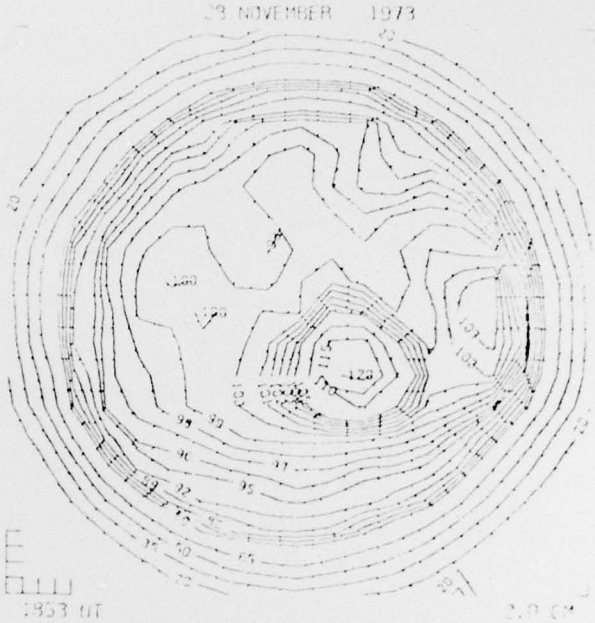


Figure 2. Radio map at 2.0 cm (1853 UT).

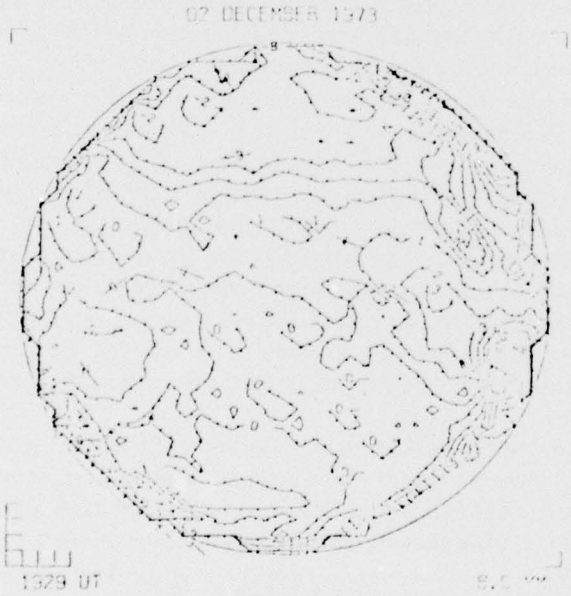


Figure 3. Differenced map.

diameter and antenna parameters, some uncertainties are produced near the limb; however, the features we are looking for are significant enough to appear in spite of this. In order to improve the limb results, a differenced quadrant was produced by subtracting the mirror image of the northwest quadrant from the northeast quadrant. Contours were then plotted only above the +5% level.

To verify the identity of features, the set of figures 4 through 7 was prepared. The Sacramento Peak Observatory $H_\alpha$ photographs have superimposed on them transparencies showing the differenced radio maps at 8.6 mm. The lower panel is the normal exposure used to show disc features while the upper panel is overexposed to bring out limb structure. In figure 4, the filament we are interested in is near the central meridian at about 40°N latitude. The deepest contour shows a depression of slightly more than −3%. On 2 and 3 December, the filament moved to the limb, as seen in figures 6 and 7. The contours in the upper panel show the prominence as a +14% enhancement. Figure 8 has been prepared to show the characteristics of the filament/prominence we are concerned with.

## MODELS AND DATA INTERPRETATION

The simplest model used to describe the radio (mm and low cm) observations of ments assumes absorption of radio waves originating in the chromosphere by the cooler, ser filament in the corona. Kundu[8] attempts to derive estimates of $T_e$ and $N_e$ by looking at the mean optical depth, $\tau = K\ell$, where K is the absorption coefficient and $\ell$ the dimension of the filament through which the radio waves must pass. The dependence of K on $T_e$ and $N_e$ allows either to be determined if the other is known or, if one observes at two wavelengths, $T_e$ and $N_e$ can be determined without assumptions, according to Kundu. Further, as one goes to longer wavelengths (higher in the solar atmosphere) the amount of absorption should decrease as a larger fraction of the radiation comes from above the filament. This same model allows independent determination of $T_e$ and $N_e$ if the filament is seen in both emission and absorption provided the filament is optically thick.[2] The electron temperature is then the same as the brightness temperature.

The radiative transfer equation for the filament on the disc can be written

$$T_B(\text{disc}) = T_\beta e^{-\tau_F - \tau_\alpha} + T_F e^{-\tau_\alpha} + T_\alpha \qquad (1)$$

where the parameters are illustrated in figure 9a and defined as follows:

$T_B(\text{disc})$ = observed brightness temperature of the filament on the disc,

$T_\beta e^{-\tau_F - \tau_\alpha}$ = brightness temperature contribution from below filament,

$T_F e^{-\tau_\alpha}$ = brightness temperature contribution from the filament,

$T_\beta e^{-\tau_\alpha}$ = brightness temperature contribution from below the altitude of the filament in the absence of a filament,

$T_F$ = brightness temperature of the filament,

$\tau_F$ = optical thickness of the filament, and

$\tau_\alpha$ = optical thickness of the region above the filament.

8. Kundu, MR, Solar Physics, 13, p 348-356, 1970

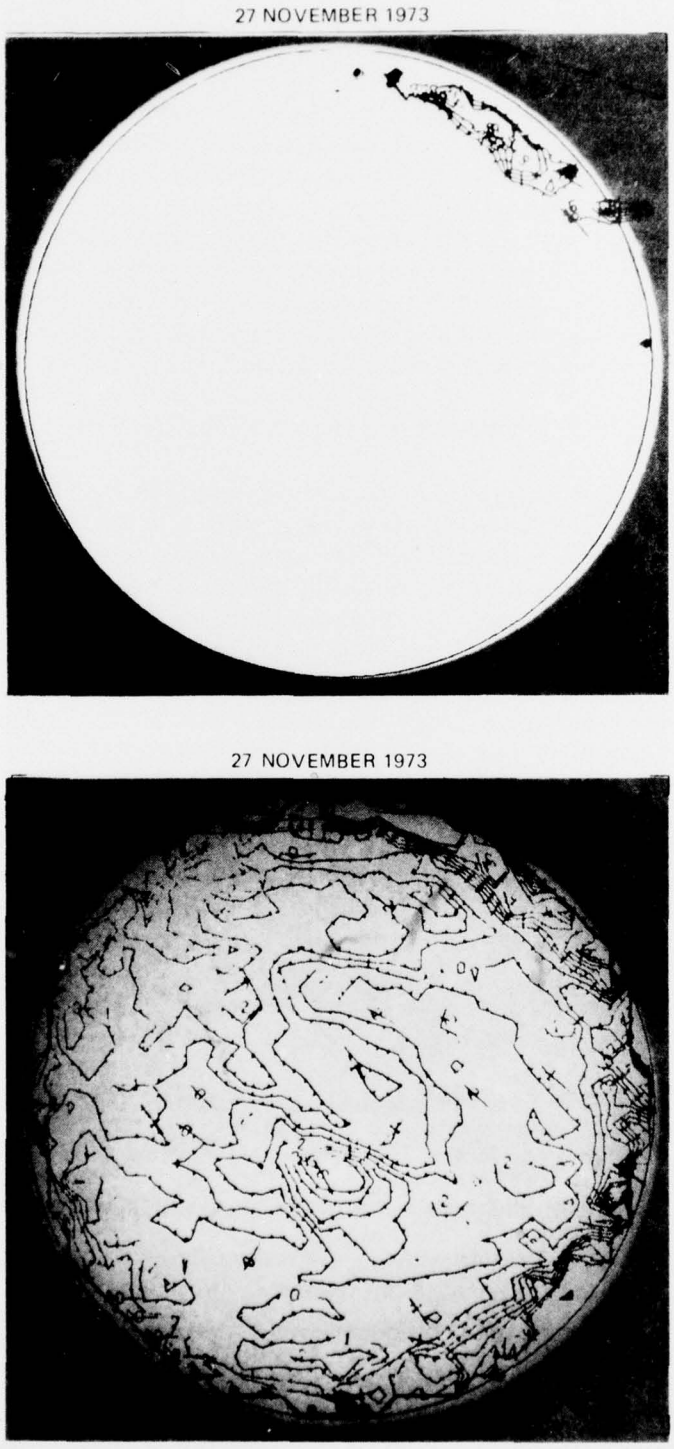


Figure 4. Differenced map at 8.6 mm showing filament near central meridian, 27 November.

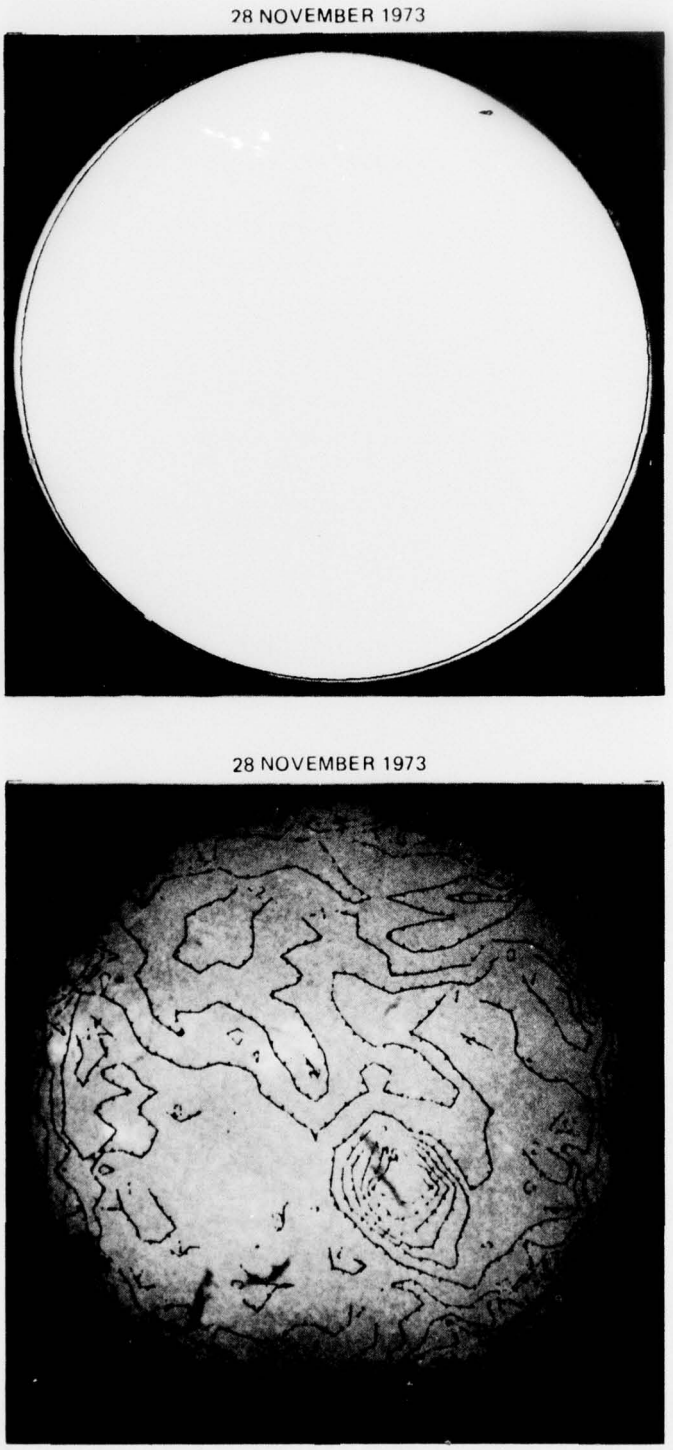


Figure 5. Differenced map at 8.6 mm, 28 November.

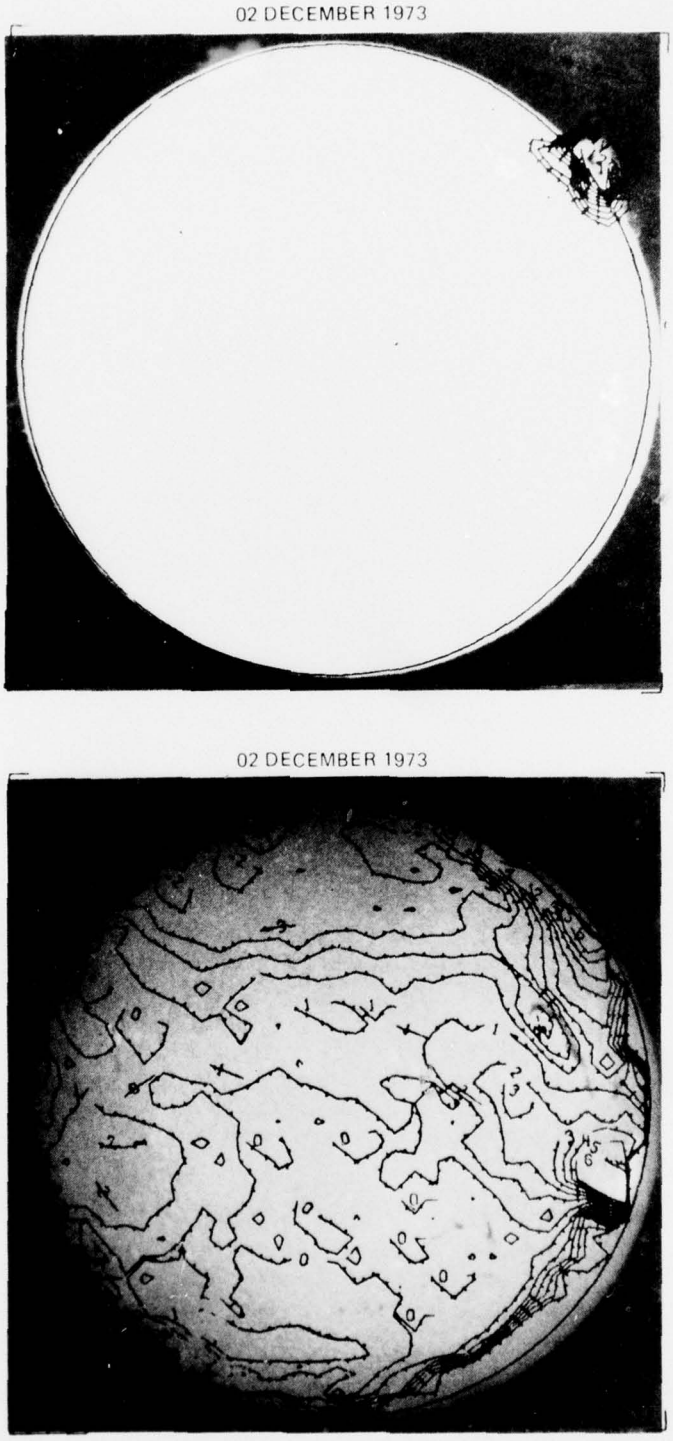


Figure 6. Movement of filament to the limb, 2 December.

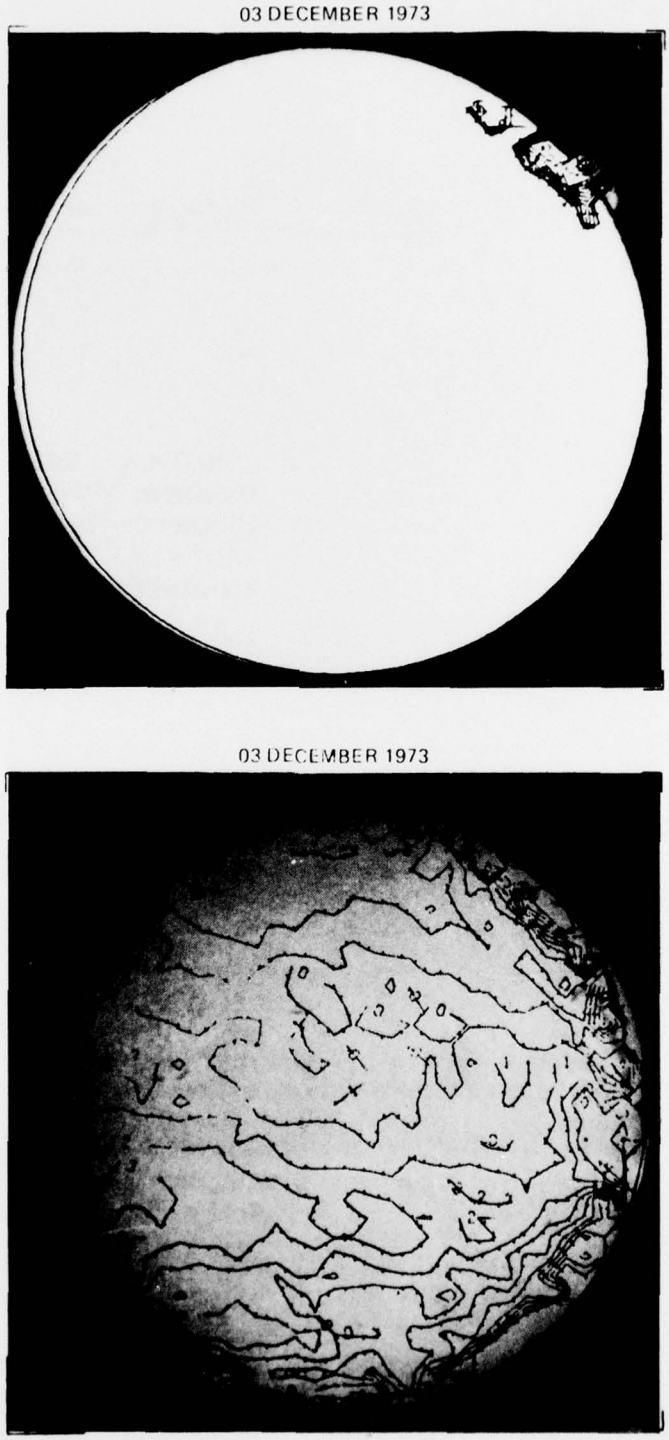


Figure 7. Movement of filament to the limb, 3 December.

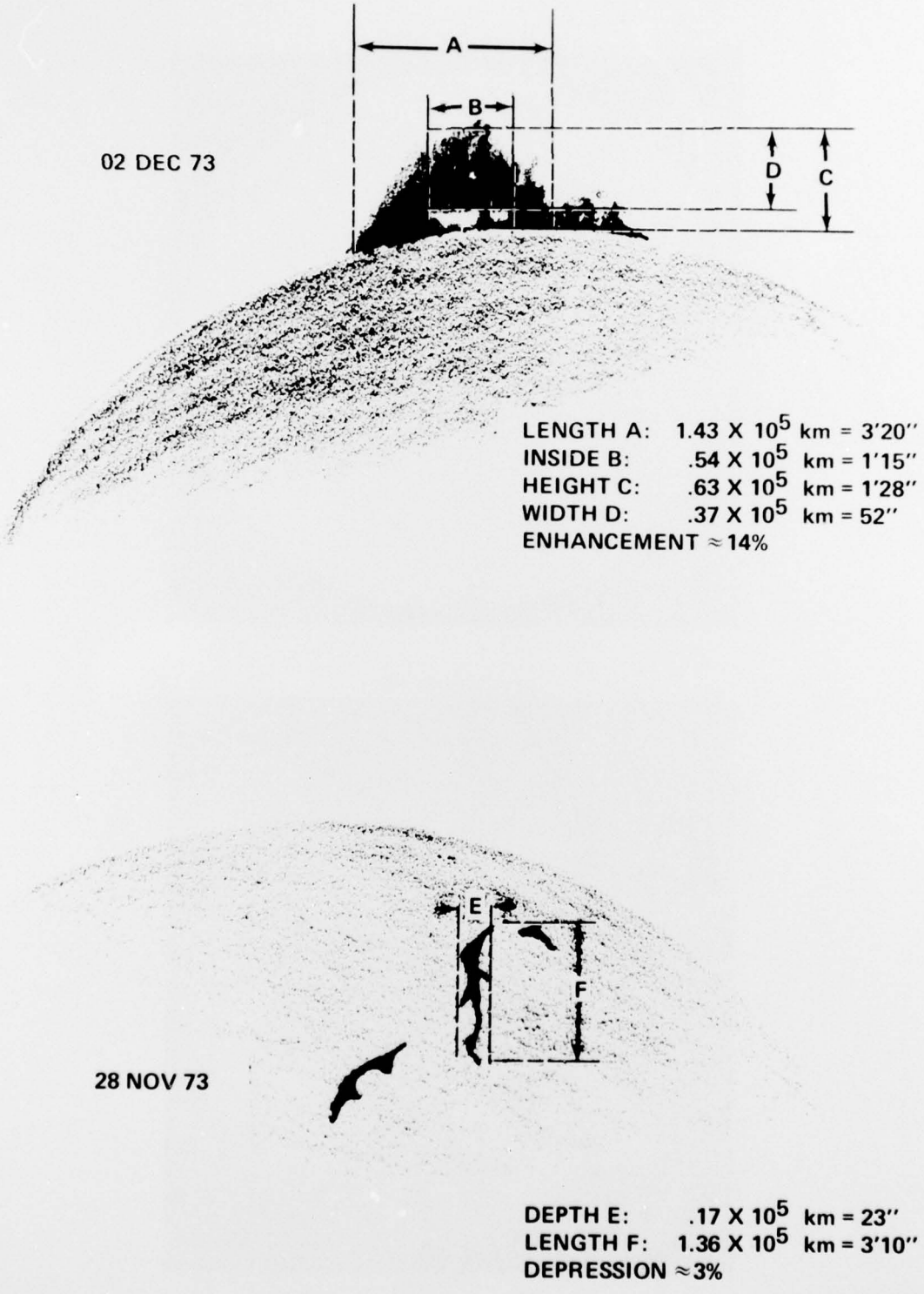


Figure 8. Filament/prominence characteristics.

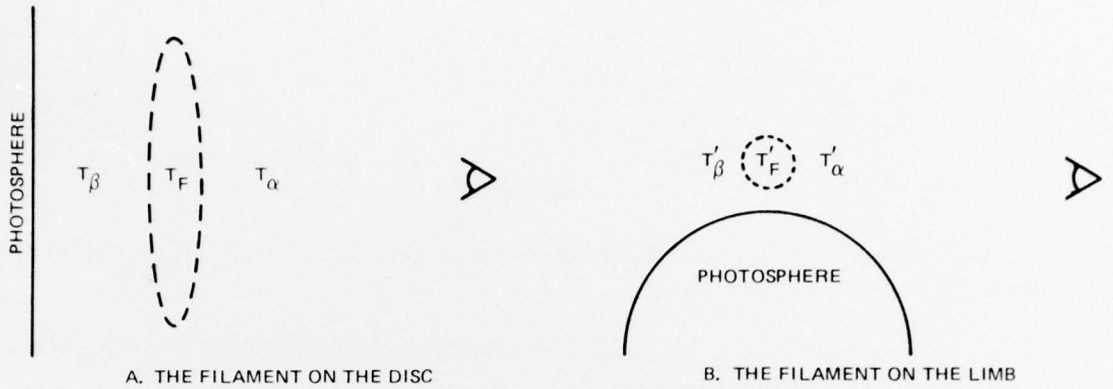


Figure 9. Filament on the disc and on the limb.

Because the filament is smaller than the beamwidth of the antenna, what is actually observed is an antenna temperature, $T_{disc}$, which is a combination of the brightness temperatures of the filament and the surrounding area on the sun. This antenna temperature is given by

$$T_{disc} = \frac{A}{C}(T_\beta e^{-\tau_F - \tau_\alpha} + T_F e^{-\tau_\alpha} + T_\alpha) + \frac{B}{C}(T_\beta e^{-\tau_\alpha} + T_\alpha) \quad (2)$$

where

C = antenna beam area = $\pi \left(\frac{FWHM}{2}\right)^2$ (rad$^2$),

A = projected filament area (rad$^2$), and

B = C–A (remaining area) (rad$^2$).

The first term on the right-hand side of equation (2) represents the contribution of $T_{disc}$ from the filament while the second term accounts for the contribution of that portion of the antenna beam not on the filament but looking at the surrounding area.

For the limb observation, the same equations hold with the exception that the notation requires modification to account for the differences between the disc and limb conditions. The radiative transfer equation is

$$T_B(\text{limb}) = T'_\beta e^{-\tau'_F - \tau'_\alpha} + T'_F e^{-\tau'_\alpha} + T'_\alpha \quad (3)$$

and the resulting antenna temperature is

$$T_{limb} = \frac{A'}{C} (T_\beta e^{-\tau'_F - \tau'_\alpha} + T'_F e^{-\tau'_\alpha} + T'_\alpha) \qquad (4)$$

$$+ \frac{B'}{C} (T'_\beta e^{-\tau'_\alpha} + T'_\alpha) .$$

The primes denote the limb symbol for the equivalent disc symbol. These are illustrated in figure 9b. It should be noted that

(a) $\tau_F$ is primed ($\tau'_F$) for the limb because $\tau \approx k\ell$ and $\ell$ is not the same for the disc and limb observations.

(b) C is not primed in equation (4) because the beamwidth remains unchanged.

The observations made at LPAO have been reduced to the difference between the individual map and the background average. Solving for this difference using equation (2) gives:

$$\Delta T_{disc} = \left[ \frac{A}{C} (T_\beta e^{-\tau_F - \tau_\alpha} + T_F e^{-\tau_\alpha} + T_\alpha) + \frac{B}{C} (T_\beta e^{-\tau_\alpha} + T_\alpha) \right] \qquad (5)$$

$$- \left[ \frac{A}{C} (T_\beta e^{-\tau_\alpha} + T_\alpha) + \frac{B}{C} (T_\beta e^{-\tau_\alpha} + T_\alpha) \right] .$$

A similar equation results from using equation (4). Equation (5) may be simplified to

$$\Delta T_{disc} = \frac{A}{C} (T_\beta e^{-\tau_F - \tau_\alpha} - T_\beta e^{-\tau_\alpha} + T_F e^{-\tau_\alpha}) , \qquad (6)$$

where again a similar equation holds for the limb case. For the reason that[9] $\tau_\alpha \ll 1$, equation (6) can be simplified again to

$$\Delta T_{disc} = \frac{A}{C} (T_\beta e^{-\tau_F} - T_\beta + T_F) . \qquad (7)$$

Assuming a constant temperature and electron density throughout the radio filament and using

$$T_F = T_e (1 - e^{-\tau_F})$$

where $T_e$ is the electron temperature in the radio filament, we can rewrite equation (7) as

$$\Delta T_{disc} \frac{A}{C} = (T_e - T_\beta)(1 - e^{-\tau_F})$$

or

$$T_e = \frac{\Delta T_{disc} C}{(1 - e^{-\tau_F})A} + T_\beta . \qquad (8)$$

9. Aerospace Corporation Report ATR-73 (8102)-8, On the Source of the Slowly Varying Component at Centimetre and Millimetre Wavelengths, by FI Shimabukuro, GA Chapman, EB Mayfield, and S Edelson, 15 Feb 73

An almost identical equation obtains for the limb case; namely,

$$T_e = \frac{\Delta T_{limb}\, C}{(1 - e^{-\tau'_F})\, A'} + T'_\beta . \qquad (9)$$

Equations (8) and (9) can be solved in four ways to obtain $T_e$ and $\tau_F$ (or $\tau'_F$) or $N_e$ because (see eq (11))

$$\tau(\lambda_1) = \tau(\lambda_2) \frac{\lambda_1^2}{\lambda_2^2} , \qquad (10)$$

which allows the following solutions:

(a) equation (8) at both wavelengths,

(b) equation (9) at both wavelengths,

(c) equations (8) and (9) at 8.6 mm, and

(d) equations (8) and (9) at 2.0 cm.

However, some of these cases are easier to solve for than others because $T_\beta \neq T'_\beta$ and $T'_\beta$ is difficult to ascertain due to its variation with radial distance near the limb. On the disc, $T_\alpha + T_\beta = T_C$ (8880K at 8.6 mm; 10900K at 2.0 cm) and because of the great height of the filament $T_\alpha \approx 0$; hence, we know $T_\beta$ at each wavelength and we can solve case (a). Table 1 lists the values of the parameters used to solve equation (8). The technique employed was one of trial and error on the optical depth. Also, because the value of the projected filament area is uncertain due to the possible noncoincidence of the size and position of the radio and optical filament, the value of A was allowed to vary.

TABLE 1. PARAMETERS FOR THE SOLUTION OF $T_e$.

| $\lambda$ | C | $\Delta T_{disc}$ | $T_\beta = T_C$ |
|---|---|---|---|
| 8.6 mm | 6.158 | -0.03 $T_C$ | 8880 K |
| 2.0 cm | 12.566 | -0.03 $T_C$ | 10900 K |

The technique used to solve for $T_e$ and $N_e$ was as follows:

1. Choose a value of A.
2. Solve equation (8), varying $\tau'_F$ (using equation (10) to relate $\tau'_F$ (8.6 mm) and $\tau'_F$ (2.0 cm) until $T_e$ (8.6 mm) = $T_e$ (2.0 cm) is achieved).

3. $N_e$ was then solved for using[10]

$$\tau_F = C\lambda^2 N_e^2 T_e^{-1.5} \Delta S \qquad (11)$$

or

$$N_e = \left( \frac{\tau_F T_e^{1.5}}{C\lambda^2 \Delta S} \right)^{1/2} \quad . \qquad (12)$$

where

$\Delta S = 37 \times 10^{-3}$ km (see length D in figure 8)

$\lambda = 8.6$ mm

$T_e$ = determined from step 2

$C = 2.2 \times 10^{-22}$ cgs units

4. Go to step 1 until a complete range of the values of A has been explored.

## RESULTS AND DISCUSSION

Figures 10–12 are plots of $T_e$, $N_e$, and $\tau_F$ (8.6 mm) as a function of the ratio A/C at 8.6 mm. It should be noted that because for $A/C > 0.2$ there is no solution to the equation, the ratio A/C cannot exceed this value. A lower limit is also arrived at because, for $A/C \lesssim 0.065$, the solution yields negative values of $T_e$. These two limits yield the following limits on $N_e$ and $T_e$, as obtained from figures 10 and 11:

$$1 \times 10^9 \lesssim N_e \lesssim 2 \times 10^{10} \text{ cm}^{-3}$$
$$5 \times 10^2 \lesssim T_e \lesssim 7.5 \times 10^3 \text{ K} \quad . \qquad (13)$$

The upper limit of A/C would obtain if the width of the filament were approximately 1.7 times that observed optically. Due to the irregular shape of the filament (see figure 8), it is difficult to ascertain the true optical area. However, using graphical techniques, it has been estimated that A/C (8.6 mm) is approximately 0.12 if the optical and radio filaments coincide. This yields the following estimates for $N_e$ and $T_e$ (from figures 10 and 11):

$$N_e \approx 7.9 \times 10^9 \text{ cm}^{-3}$$
$$T_e \approx 5300 \text{ K} \quad . \qquad (14)$$

## TWO-COMPONENT MODELS

In the above analysis we have assumed that the radio filament, by which we mean that structure in the solar atmosphere responsible for the observed change in antenna temperature, has a uniform temperature and density. This is obviously not correct, but it represents a good

10. Allen, CW, Astrophysical Quantities, The Athlove Press, University of London, 1963

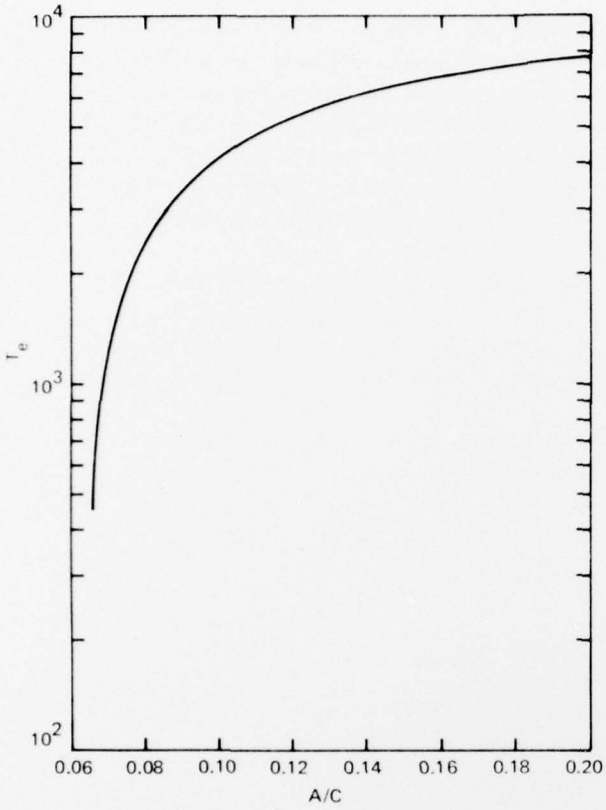


Figure 10. Electron temperature as a function of the parameter A/C where the value of C is determined for 8.6-mm wavelength.

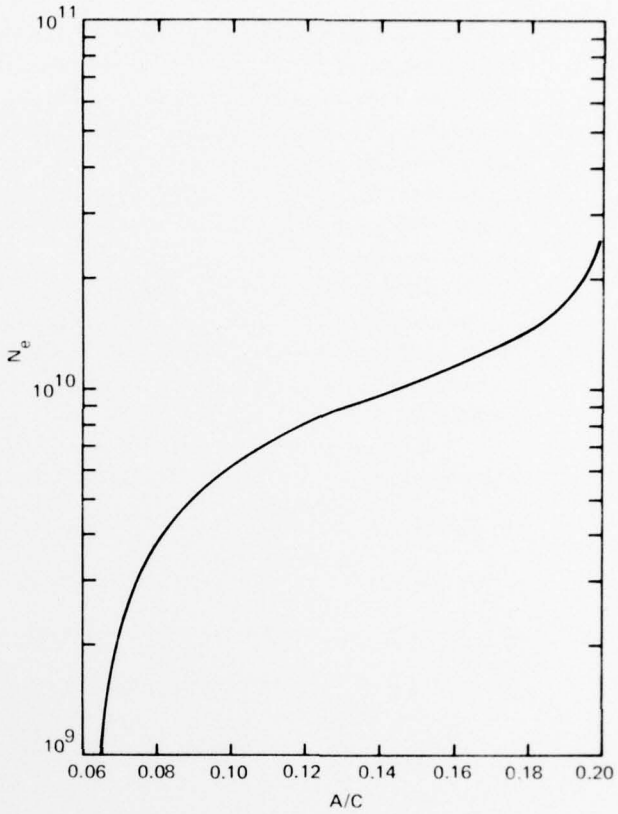


Figure 11. Electron density as a function of the parameter A/C where the value of C is determined from 8.6-mm wavelength.

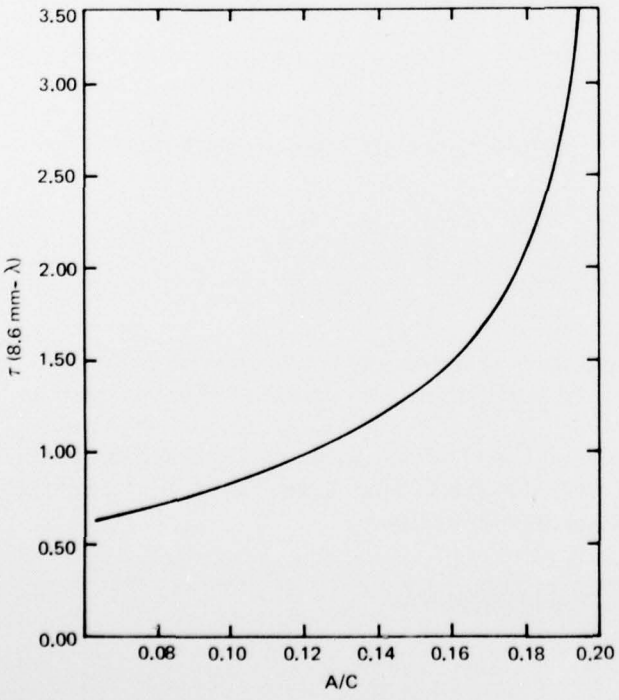


Figure 12. Optical depth at 8.6-mm wavelength as a function of the parameter A/C where the value for C is determined from 8.6-mm wavelength.

initial model. In recent papers, Straka[4] and Butz[6] use two-component models in analyzing radio filament data. Both models combine a dense, cool filament surrounded by an optically thin transition layer; however, they differ in the relative sizes of the two components. In the Butz model,[6] which is similar to that discussed by Simon and Wickstrom,[11] the filament is surrounded by a sheath which is both optically thin and physically thin. In terms of projected area, the sheath occupies only about 0.1 the area of the filament. Within this thin sheath, the temperature rises from that of the cool filament to the ambient temperature of approximately $10^6$ K.

In the Straka model,[4] the filament is surrounded by a cavity which is optically thin but physically quite large. In terms of projected area, the cavity occupies about 10 times the area of the filament. They conclude that if the temperature structure inside the cavity is the same as in the surrounding atmosphere, the electron density must be lower than ambient by a factor of two.

We can get an idea of the effect of this more complicated structure by a slight modification of the analysis. If we define the following parameters:

$A_1$ = projected area of the filament in the antenna beam,

$A_2$ = projected area of the cavity or sheath apart from $A_1$,

$\tau_{F1}$ = optical thickness in area $A_1$,

$\tau_{F2}$ = optical thickness in area $A_2$,

$T_{F1}e^{-\tau\alpha}$ = brightness temperature contribution from $A_1$, and

$T_{F2}e^{-\tau\alpha}$ = brightness temperature contribution from $A_2$,

then for disc observations, the differenced map shows

$$\frac{\Delta T_{disc}}{T_\beta} \approx \frac{A_1}{C}\left[\frac{T_{F1}}{T_\beta} - (1-e^{-\tau_{F1}}) + \frac{A_2}{C}\,\frac{T_{F2}}{T_\beta} - (1-e^{-\tau_{F2}})\right] . \qquad (15)$$

Again making the simplifying assumption of uniform temperature and density within each component, we obtain

$$T_{e1} \approx \frac{\Delta T_{disc}\, C}{(1-e^{-\tau_{F1}})A_1} + T_\beta - \left\{\frac{A_2}{A_1}(T_{e2}-T_\beta)\left[\frac{T_{F2}}{1-e^{-\tau_{F1}}}\right]\right\} , \qquad (16)$$

where $T_{e1}$ and $T_{e2}$ are the effective temperatures of the respective components. Note that reducing the thickness of the sheath/cavity to zero gives us back equation (8) for the one-component model.

In the case of the thin sheath model, the small optical depth ($\tau_{F2} \ll 1$) and the small thickness ($A_2/A_1 \approx 0.1$) combine to minimize the effect of the sheath. Hence, we may expect that our determinations of $T_e$ and $N_e$ are not greatly in error.

---

11. Simon, M, and Wickstrom, B, Solar Physics, 20, p 122-129, 1971

In the case of the cavity model, the small optical depth ($\tau_{F2} \ll 1$) is compensated for by the large size ($A_2/A_1 \approx 10$). Should this model prove correct, our determinations could be seriously in error. Note that because the filament may shadow a large portion of the cavity when viewed from certain angles, the optical depths $\tau_{F2}$ and $\tau_{F1}$ are related geometrically. This makes a more complete analysis of this model beyond the intended scope of this study.

## CONCLUSIONS

An analysis of the observations based on the simple one-component filament model has yielded a temperature and electron density which seem reasonable. One thing which impressed the authors is the relatively small number of radio filament observations which have been analyzed. It would seem wise to base our knowledge of radio filaments on a larger statistical sample than has been thus far utilized. In view of the success of the analysis based on disc observations at two wavelengths presented above, we believe that a more comprehensive filament study using the LPAO radioheliograms is indicated.

## REFERENCES


1. Khangil'din, UV, Soviet Astronomy-AJ, 8, p 234-242, 1964

2. Kundu, MR, Solar Physics, 25, p 108–115, 1972

3. Kundu, MR, and McCullough, TP, Solar Physics, 24, p 133–141, 1972

4. Straka, RM, Papagiannis, MD, and Kogut, JA, Solar Physics, 45, p 131–149, 1975

5. Chiuderi-Drago, F, Furst, E, Hirth, W, and Lantos, P, Astronomy and Astrophysics, 39, p 429–434, 1975

6. Butz, M, Furst, E, Hirth, W, and Kundu, MR, Solar Physics, 45, p 125–129, 1975

7. Megatek Corporation Report R2005-031-IF-3, by FL Wefer, 5 April 1976

8. Kundu, MR, Solar Physics, 13, p 348–356, 1970

9. Aerospace Corporation Report ATR-73, On the Source of the Slowly Varying Component at Centimetre and Millimetre Wavelengths, by FI Shimabukuro, GA Chapman, EB Mayfield, and S Edelson, 15 February 1973

10. Allen, CW, Astrophysical Quantities, The Athlove Press, University of London, 1963

11. Simon, M, and Wickstrom, B, Solar Physics, 20, p 122–129, 1971